



**HAL**  
open science

## Simple elaboration of drug-SPION nanocapsules (hybridosomes®) by solvent shifting: effect of the drug molecular structure and concentration

Déborah Iglicki, Myrtil L Kahn, Clément Goubault, Marielle Blot, Ulrich Jarry, Rémy Pedeux, Rémy Le Guével, Soizic Chevance, Fabienne Gauffre

► **To cite this version:**

Déborah Iglicki, Myrtil L Kahn, Clément Goubault, Marielle Blot, Ulrich Jarry, et al.. Simple elaboration of drug-SPION nanocapsules (hybridosomes®) by solvent shifting: effect of the drug molecular structure and concentration. *International Journal of Pharmaceutics*, 2024, 649, pp.123645-123645. 10.1016/j.ijpharm.2023.123645 . hal-04328696

**HAL Id: hal-04328696**

**<https://hal.science/hal-04328696>**

Submitted on 30 May 2024

**HAL** is a multi-disciplinary open access archive for the deposit and dissemination of scientific research documents, whether they are published or not. The documents may come from teaching and research institutions in France or abroad, or from public or private research centers.

L'archive ouverte pluridisciplinaire **HAL**, est destinée au dépôt et à la diffusion de documents scientifiques de niveau recherche, publiés ou non, émanant des établissements d'enseignement et de recherche français ou étrangers, des laboratoires publics ou privés.



Distributed under a Creative Commons Attribution - NonCommercial 4.0 International License

# Simple elaboration of drug-SPION nanocapsules (hybridosomes<sup>®</sup>) by solvent shifting: effect of the drug molecular structure and concentration

Déborah Iglücki<sup>1</sup>, Myrtil L. Kahn<sup>2</sup>, Clément Goubault<sup>1</sup>, Marielle Blot<sup>1</sup>, Ulrich Jarry<sup>3-4</sup>, Rémy Pedoux<sup>3-5</sup>, Rémy Le Guével<sup>6</sup>, Soizic Chevance<sup>1</sup> and Fabienne Gauffre<sup>1\*</sup>

<sup>1</sup>Univ Rennes, CNRS, ISCR-UMR6226, F-35000 Rennes, France

<sup>2</sup>LCC, CNRS, Toulouse F-31000, France

<sup>3</sup>Univ Rennes, CNRS, INSERM, BIOSIT UAR 3480, US\_S 018, Oncotrial, F-35043 Rennes, France

<sup>4</sup>Biotrial Pharmacology, Unité de Pharmacologie Préclinique, Rennes, France.

<sup>5</sup>Univ Rennes, INSERM, OSS (Oncogenesis Stress Signaling), UMR\_S 1242, CLCC Eugène Marquis, F-35042, Rennes, France

<sup>6</sup>Univ Rennes, CNRS, INSERM, BIOSIT UAR 3480, US\_S 018, Impacell, F-35043 Rennes, France

**Abstract:** Drug nanocapsules coated with iron oxide nanoparticles (SPION) were elaborated by the simultaneous nanoprecipitation of the drug and the nanoparticles, through solvent shifting. We examined four drugs: sorafenib, sorafenib tosylate,  $\alpha$ -tocopherol and paclitaxel, to cover the cases of molecular solids, ionic solids, and molecular liquids. We first investigated the formation of the drug core in the final mixture of solvents at different concentrations. A Surfactant Free Micro-Emulsion domain (SFME, thermodynamically stable) was observed at low drug concentration and an Ouzo domain (metastable) at high drug concentration, except for the case of paclitaxel which crystallizes at high concentration without forming an Ouzo domain. When co-nanoprecipitated with the molecular drugs in the Ouzo domain (sorafenib or  $\alpha$ -tocopherol), the SPION limited the coalescence of the drug particles to less than 100 nm, forming capsules with a drug encapsulation efficiency of ca 80 %. In contrast, larger capsules were formed from the SFME or when using the ionic form (sorafenib tosylate). Finally, the sorafenib-SPION capsules exhibit a similar chemotherapeutic effect as the free drug on the hepatocellular carcinoma in vitro.

**Keywords:** Solvent shifting; Nanoprecipitation; Pickering emulsions; Nanocapsules; Ouzo effect

## 1. Introduction

The design of nanocapsules with a controlled architecture remains a major scientific and technological objective to this day.<sup>1</sup> In particular, in the field of drug delivery it is desirable that the therapeutic molecule forms a dense core, to optimize its concentration per particle.

Size issues are also critical.<sup>2</sup> Hence, for systemic delivery, particles should preferably be in between 10 and 200 nm, smaller particles being too rapidly excreted and larger ones more easily recognized and eliminated by the immune system.<sup>3,4</sup> The protecting shell is generally needed to provide dispersability and colloidal stability and sometimes more elaborate features such as stealth, targeting, responsiveness to stimuli... Polymers and polymeric surfactants have been widely used for this purpose, as they can be designed to play all these roles. Capsule shells made of inorganic nanoparticles, where the nanoparticles impart an additional specific therapeutic function such as MRI or photoacoustic imaging, radiosensitization or photothermal therapy, have also been described.<sup>5-8</sup>

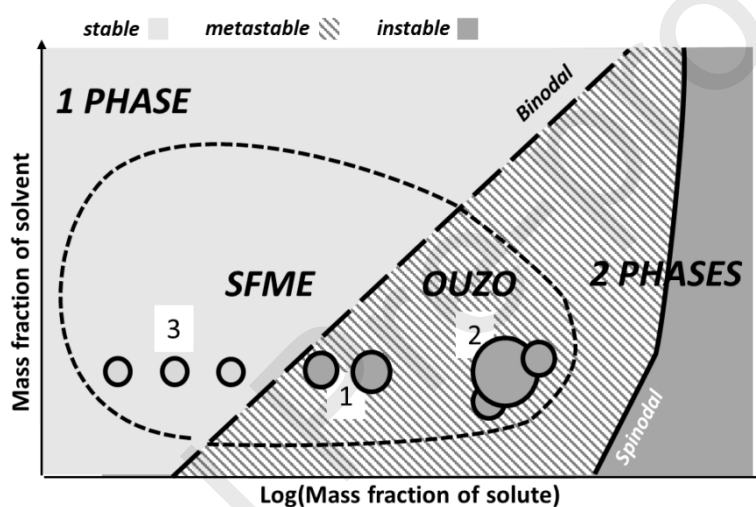


Figure 1: Schematic representation of the SFME and Ouzo domains of a ternary system water/solvent/solute, using a 2D composition plot. mass fraction of water = 1-mass fraction of (solvent+ solute). Numbers 1-3 correspond to (1) monodisperse Ouzo droplets; (2) polydisperse Ouzo droplets and (3) surfactant-free microemulsion (SFME) particles, as stated in text.

Nanoprecipitation and emulsion-evaporation are the techniques allowing the highest payloads, since in these cases the core can be made of 100% of the compound of interest. In particular, drug nanoprecipitation is widely used for the preparation of therapeutic nanoparticles. Among the various methods of nanoprecipitation, the solvent displacement method is often preferred because it requires very little energy. In this method, a solute initially dissolved in a good solvent precipitates on addition of a non-solvent. The solvent and non-solvent should be miscible. A protective shell of polymer or nanoparticles can also be deposited by co-nanoprecipitation, either simultaneously or sequentially.<sup>1,7,9-11</sup> The supersaturation rate, which depends both on the solvent composition and on the solute concentration, plays a major role in nanoprecipitation by solvent displacement. Several situations are observed depending on the zone of the compositions space where the nanoprecipitation is performed (Figure 1).<sup>12-15</sup> (1) Small and weakly polydisperse particles are formed in the Ouzo domain, a domain generally quite restricted near the solubility limit or

“binodal” line. As this is a metastable domain, the particles evolve more or less slowly, possibly via coalescence or Ostwald ripening.<sup>16–18</sup> (2) At higher solute or non-solvent concentrations (higher supersaturation) a polydisperse population of fast-growing particles is observed. (3) Particles also form in a region of the single-phase domain, called surfactant free microemulsion (SFME). These are very homogeneous in size and not evolving over time. Note that the existence of this micro-emulsion cannot be explained in the framework of nanoprecipitation, since in this domain, the solute concentration is lower than its solubility limit. An explanation is not available yet, but we see it as analogous to micelles and microemulsions of surfactant systems. In a recent paper,<sup>19</sup> we presented a methodology to elaborate phase diagrams of Ouzo systems using a combination of Static Multiple Light Scattering (SMLS, to probe stability) and Nanoparticle Tracking Analysis (NTA, to quantify polydispersity). This allows to discriminate unambiguously between the SFME, Ouzo, and polydisperse Ouzo “states”.

Both the SFME and Ouzo domains are of interest to prepare nanocapsules.<sup>9,10,20–22</sup> Thus, Bernard and Ganachaud showed that it was possible to form polymer-coated oil capsules by using a polymer whose precipitation domain overlaps either the SFME or the Ouzo domain of the oil.<sup>21,10</sup> In their work, the solvent mixture used is water/acetone and the oil is either hexadecane or Miglyol, and the polymer is a rather water-soluble glycopolymer. The polymer does not appear to alter the water/acetone/oil diagram.

More recently, our team prepared nanocapsules coated with nanoparticles by nanoprecipitating a hydrophobic solute, butylated hydroxytoluene (BHT), in water/THF mixtures in the presence of hydrophobic nanoparticles. Although this solute is solid in the pure state at room temperature, the objects formed in the Ouzo domain contain solvent and remain partially liquid.<sup>19</sup> Interestingly, the presence of nanoparticles limits the coalescence of Ouzo emulsions and can significantly focus their distribution.<sup>23</sup> This phenomenon, initially described in the case of Pickering emulsions,<sup>24,25</sup> induces a stabilization of the droplets, and consequently a widening of the Ouzo domain, towards high solute concentrations. The cross-linking of the nanoparticle shell by a polymer confers a very high mechanical stability to the capsules thus formed, which were named “hybridosomes”.<sup>7,26</sup>

This strategy is very attractive for the elaboration of nanocapsules of nanoparticles, containing drugs, for therapeutic applications.<sup>27</sup> It is possible to dissolve the therapeutic molecule of interest in the oil forming the core of the capsule.<sup>28</sup> However, since many therapeutic molecules are hydrophobic, it seems more favorable that the core of the capsule is entirely made of them. In addition to a very high stability, nanoparticles can bring additional specific properties to the nanocapsules. We have previously demonstrated that hybridosomes made of superparamagnetic iron oxides are MRI contrast agents as efficient as commercial agents such as Feraspin<sup>TM</sup>.<sup>7</sup> When their shell contains gold nanoparticles, the hybridosomes are effective radiosensitizers, allowing to potentiate radiotherapy.<sup>8</sup>

Herein, we investigated the formulation of capsules using the cargo of interest as the organic core. Four hydrophobic drugs with various physico-chemical properties: paclitaxel, sorafenib

(both molecular solids), sorafenib tosylate (ionic solid), and  $\alpha$ -tocopherol (molecular liquid). The concentrations were varied to cover both the SFME and Ouzo domains and the cytotoxic effect of sorafenib-loaded hybridosomes was quantified in vitro.

## 2. Materials and methods

**Materials. Synthesis.** Superparamagnetic iron oxide nanocrystals (SPION) ( $\gamma$ -Fe<sub>2</sub>O<sub>3</sub>; mean diameter 5 nm) were synthesized following a reported procedure, using octylamine (2 eq.) and oleic acid (1eq.) as ligand and no additional solvent.<sup>29</sup> Tetrahydrofuran (THF, inhibitor-free, HPLC grade,  $\geq 99.9\%$ ) was purchased from Sigma-Aldrich and dried over a solvent purification system. ( $\pm$ )  $\alpha$ -tocopherol (vitamin E) from BASF was graciously provided by AMI-ingredient. Paclitaxel ( $> 98\%$ ) was purchased from TCI, sorafenib ( $\geq 98\%$ , HPLC grade) and sorafenib tosylate ( $\geq 98\%$ , HPLC grade) from Sigma-Aldrich. Butylated hydroxytoluene (BHT) was purchased from Janssen. Samples were made using MilliQ water (18.2 M $\Omega$ .cm). Poly(ethylene glycol)-*b*-poly(acrylic acid) ( $M_{\text{PEG}} = 2$  kDa;  $M_{\text{PAA}} = 7.2$  kDa) were kindly provided by G. Casterou. **HPLC analysis.** Acetonitrile (ACN, HPLC grade,  $\geq 99.8\%$ ) and water (HPLC Gradient grade) were purchased from Fisher Chemical, and water-free (glacial) acetic acid from CARLO ERBA Reagents.

**Sample preparation by nanoprecipitation. Samples without nanoparticles.** Samples were prepared by adding water to a THF solution of the hydrophobic solute ( $\alpha$ -tocopherol, sorafenib, sorafenib tosylate or paclitaxel). Addition is achieved in one-shot using a micropipette and the sample is vortexed for ca 10 s except for SMLS analysis. **Hybridosomes.** The samples were prepared following the same procedure, with SPION previously dispersed in the drug containing THF solution. The final  $\gamma$ -Fe<sub>2</sub>O<sub>3</sub> concentration was ca 20  $\mu\text{g}\cdot\text{mL}^{-1}$ . After 6 hours, the PEG-PAA was added at a concentration of acrylic acid units of 2.4  $\text{mmol}\cdot\text{L}^{-1}$  and the solvent was slowly evaporated overnight at 40 °C. Magnetic separation was performed twice for 24 h, the supernatant was discarded and the pellet dispersed in water. The suspension was characterized by NTA (see section below) and TEM using a JEOL 2100 LaBG electron microscope equipped with a Gatan Orius 200D camera (THEMIS, Scanmat).

**Static Multiple Light Scattering (SMLS).** A Static Multiple Light Scattering (SMLS) device (TurbiScan™ TOWER from Formulacion, France) was used to monitor the stability of the emulsions. The device measures optical transmission and back scattering over the sample height and over time using a near infrared light source ( $\lambda = 880$  nm) and two synchronous detectors that move up and down along the sample. The samples were prepared in glass vials by adding water in one shot to the organic solution. For mixing, each sample was slowly turned over 3 times and monitored for 14 h. Results are provided as the relative transmission relative to the first scan.

**Nanoparticle Tracking Analysis (NTA).** NTA was carried out using a Nanosight LM10 device (Malvern Panalytical). The sample was inserted into the cell of the device and illuminated by a laser beam (40 mW,  $\lambda = 405$  nm). The light scattered by the nano-objects appears as individual spots which trajectories are recorded by a CCD camera, operating at 30 frames per second, through a microscope. For each sample (with or without SPION), measurements were achieved a few minutes after mixing. Each measurement consists of 3 acquisitions of 30 s, at 25°C. The size of each object was then individually deduced from the analysis of its Brownian

motion (NANOSIGHT NTA 2.0 Analytical Software) using the viscosity of the appropriate solvent, i.e.  $0.9 \times 10^{-3}$  Pa.s for water or  $1.55 \times 10^{-3}$  Pa.s for the THF/water (23/77 w/w) mixture.<sup>30</sup>

**Electrophoretic mobility.** Electrophoretic mobility was measured using a Malvern Nanosizer operating at 633 nm and equipped with a dip cell (ZEN1002). The reported values represent the mean and standard deviation of three independent sets of 100 measurements.

**Encapsulation yield.** The sorafenib encapsulation yield (*EY*) was determined by HPLC (High performance liquid chromatography) assay. The chromatography system (AGILENT 1200) consisted of a gradient pump with degas option and gradient mixer, a UV detector, a manual injector and the Agilent 1260 Infinity Thermostated Column Compartments (G1316A TCC). Chromatographic separation was performed on a C18 column (4.6 mm × 150 mm, 5 μm pore size; AGILENT ZORBAX EclipseE XDB-C18 Analytical Column), using acetonitrile (A) and water containing 0.2% v acetic acid (B) as the mobile phase, at a flow rate of  $1.0 \text{ mL}\cdot\text{min}^{-1}$ , operated at 25°C with an elution gradient: from 40:60 (A:B v/v) at the injection time to 75:25 (A:B v/v) over 40 min. Then, the chromatographic system was equilibrated during 5 min before changing back to 40:60 (A:B v/v) within 5 min. The volume of the injection was 20 μL and the eluent was monitored at a wavelength of 254 nm. The retention time of the sorafenib was 18.7 min.

The calibration curve was obtained using sorafenib standard solutions in the range 0.001-0.45 mM in methanol and plotting the area under the curve of the HPLC assay (mAbsorbanceU.s) vs concentration. The slope and correlation coefficient were 34390 and 0.9957, respectively.

The *EY* was calculated as follows:

$$EY(\%) = \frac{C_{\text{soraf, ini}} - (\sum C_{\text{soraf, sup}})}{C_{\text{soraf, ini}}} \times 100$$

where  $C_{\text{soraf, ini}}$  is the concentration of sorafenib initially introduced at the beginning of the process and  $C_{\text{soraf, sup}}$  is the concentrations of sorafenib measured in the supernatants collected after each magnetization.

**Cell culture, cytotoxicity of sorafenib and cell survival assay.** Cytotoxicity assays were achieved by the ImpACcell platform in Rennes (ImpACcell / UAR BIOSIT / Rennes University). Hepatocellular carcinoma cancer cell lines HuH-7 were obtained from the ECACC collection (European Collection of Authenticated Cell Cultures, Porton Down, United Kingdom). They were modified to express luciferase as reported in a previous study<sup>8</sup> (HuH-7-Luc, no bioluminescence measurement herein). Cells were grown at 37°C, 5 % CO<sub>2</sub> in DMEM. All culture media were supplemented with 10 % fetal bovine serum (FBS), 1 % penicillin-streptomycin and 2 mM glutamine. The IC<sub>50</sub> assays were performed using sorafenib at 0.1 μM, 0.3 μM, 0.9 μM, 3 μM, 9 μM, and 25 μM (well concentrations). DMSO was used as a control treatment. Hybridosomes formulated with BHT as the organic core were used as negative control. Cells were plated in 96 wells at a number of 4000 cells/well. After 24 h, the cells were exposed to the chemotherapy and after 48 h of treatment, the cells were washed in PBS and fixed in 90/5 (v/v) ethanol/glacial acetic acid for 20 min. Nuclei were stained with Hoechst

33342 (bisBenzimide H 33342 trihydrochloride,  $\geq 98\%$  HPLC and TLC grade, reference B2261 at Sigma-Aldrich). Image acquisition and analysis to count residual cells were performed using a Cellomics ArrayScan VTI/HCS (ThermoScientific). Survival percentages are calculated as the percentage of the number of cells after treatment with compound compared to the number of cells after treatment with DMSO. Relative  $IC_{50}$  is calculated using the XLfit 5.5.0.5 (idbs) curve fit within Microsoft Excel as an add-on. The 4-parameter logistic model or sigmoidal dose-response model is used according to the following equation:

$$Fit = \frac{A - D}{1 + \left(\frac{X}{C}\right)^B} + D$$

Where *Fit* is the response, *X* is the concentration, *D* is the lower asymptote (the bottom of the curve), *A* is the upper asymptote (the top of the curve), *B* the Hill coefficient and *C* ( $IC_{50}$ ) is the concentration corresponding to the response at mid height between *A* and *D*.<sup>31</sup>

### 3. Results and discussion.

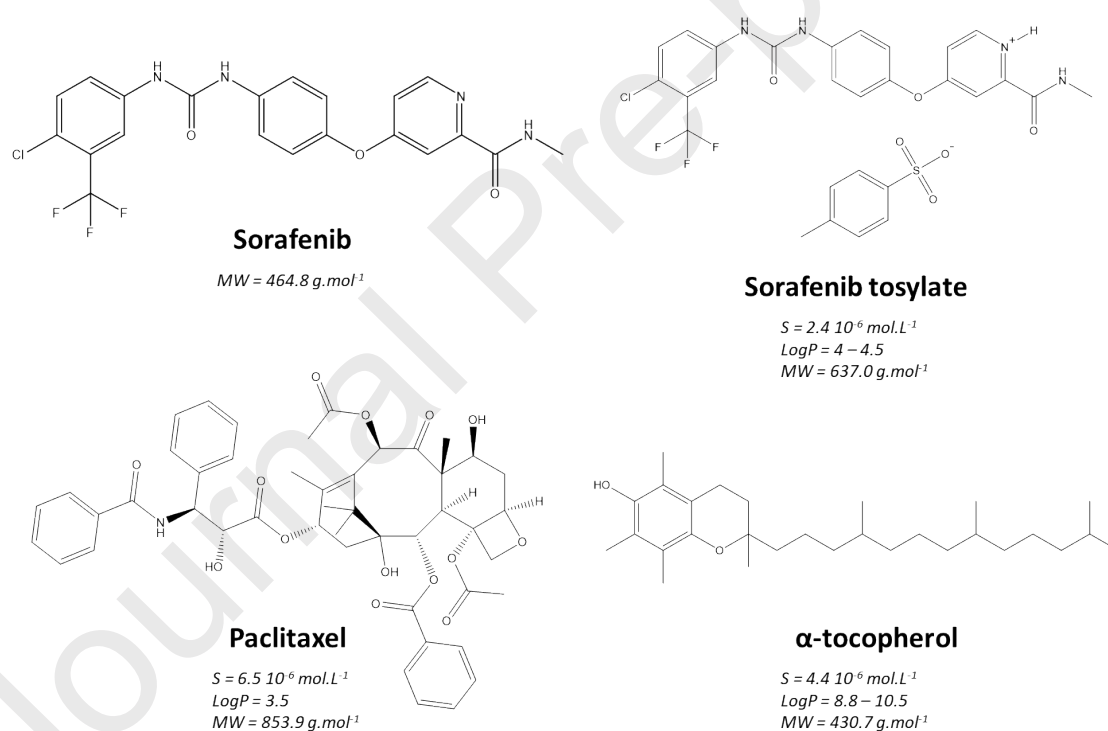


Figure 2: Molecular structures of the targeted drugs, with their molar mass (*Mw*), water solubility (*S*) and *LogP*, from Drugbank.<sup>32</sup>

We selected four therapeutic compounds: sorafenib, sorafenib tosylate, paclitaxel and  $\alpha$ -tocopherol (Figure 2). Sorafenib is a kinase inhibitor indicated for the treatment of unresectable hepatocellular carcinoma and advanced renal cell carcinoma. Sorafenib was approved for clinical use under the form of its tosylate salt, more soluble in water and other polar solvents, and orally administered as tablets of micronized particles.<sup>33–36</sup> However, both

forms are biologically active and we found it interesting to compare their processability. The water solubility and LogP values of sorafenib are not indicated in the Figure 2, because they are beyond the detection limit of conventional analytical methods, such as HPLC, and values found in some databases seemed questionable.<sup>37</sup> Paclitaxel is a mitotic inhibitor for the treatment of advanced carcinoma of the ovary, and other cancers such as breast and lung cancers.<sup>38</sup> The  $\alpha$ -tocopherol, known as “vitamin E”, is an antioxidant used as a dietary supplement. Based on our previous studies, we hypothesized that due to their low water solubility (typically below  $10^{-5}$  mol.L<sup>-1</sup>) these molecules may be precipitated to form the core of the capsules. We used superparamagnetic iron oxide nanocrystals (SPION) as the shell material. These SPION (4.8 (+/- 0.9) nm nanocrystals, coated with alkyl chains) were synthesized via the hydrolysis of  $[\text{Fe}(\text{N}(\text{SiMe}_3)_2)_2]$  in a mixture of octylamine and oleic acid in the absence of any additional solvent.<sup>23</sup> They are readily dispersible in THF and precipitate in the presence of a few percent of water, which makes them suitable for co-nanoprecipitation from any water-THF mixtures.<sup>7</sup> The superparamagnetic SPION assembled within the capsule shell exhibit a higher magnetic susceptibility than the free ones, yet allowing a convenient purification of the capsules by magnetic separation. In addition, these particles present a low cellular toxicity.<sup>7</sup>

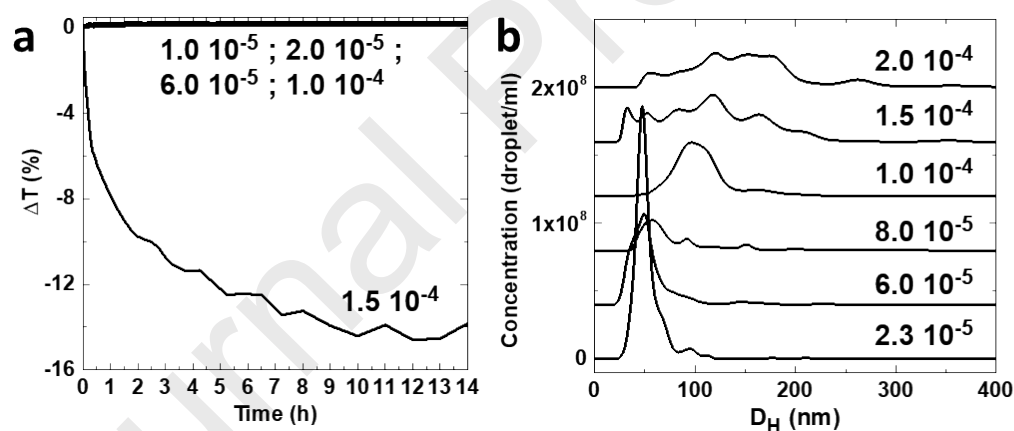


Figure 3: Characterization of samples of various sorafenib compositions (mass fractions ( $\pm 0.1$ ) as indicated on graphs) in the water/THF/sorafenib system. (a) Stability analysis using SMLS. (b) Size distribution measured using NTA.

**3.1 Case of molecular sorafenib.** We have first investigated a cross-section of the water/THF/sorafenib phase diagram (in the absence of SPION), following the methodology reported previously.<sup>19</sup> To this aim, we analyzed a series of compositions with sorafenib mass fractions in the range  $10^{-5}$  –  $2 \times 10^{-4}$ , keeping the mass fraction of THF at a constant value of 0.23 (Table SI 1). The NTA shows that all samples contain nanoprecipitated particles and their size distributions are displayed in Figure 3b. Note that the NTA measures the hydrodynamic diameter ( $D_H$ ). The samples with a sorafenib mass fraction from  $2.3 \times 10^{-5}$  to  $10^{-4}$

<sup>4</sup> exhibit a monomodal distribution (Figure 3b) and their SMLS analyses show no sign of evolution for 14 h after preparation (Figure 3a), which is the signature of a SFME. In contrast, more concentrated samples evolve over time and already exhibit a broad size distribution a few minutes after mixing. These latter samples are “polydisperse” Ouzo emulsions.

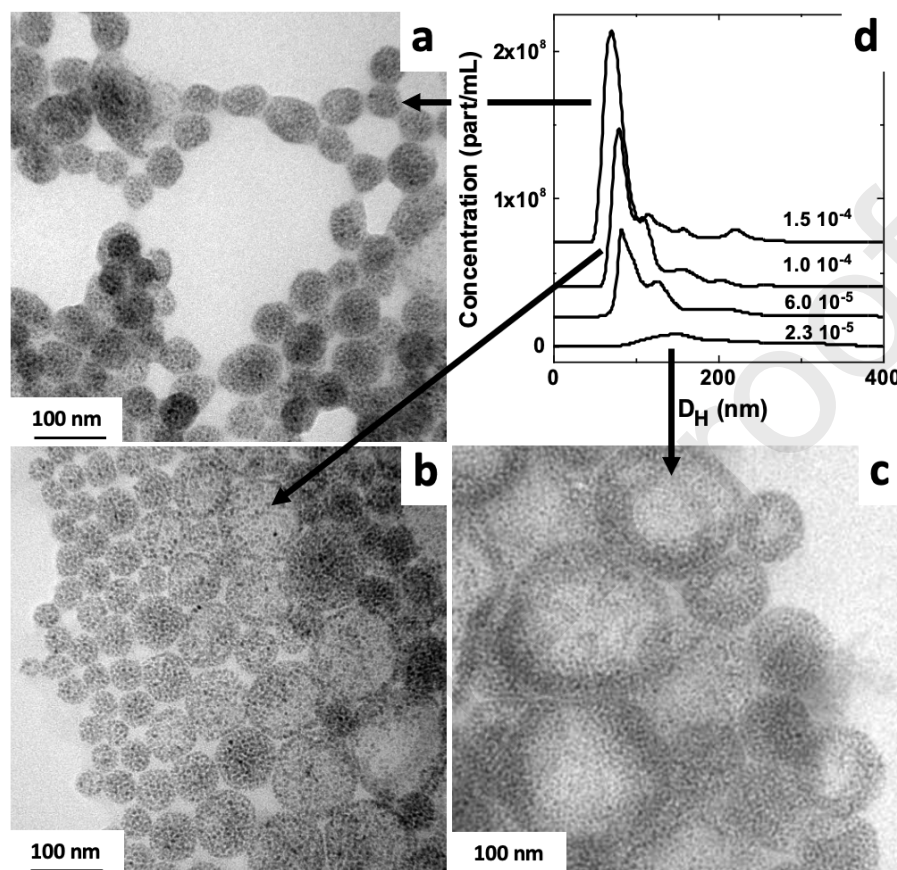


Figure 4: Characterization of sorafenib-SPION nanocapsules. (a-c) TEM pictures of the capsules for three mass fractions of sorafenib:  $2.3 \times 10^{-5}$ ,  $1.0 \times 10^{-4}$ ,  $1.5 \times 10^{-4}$ . (d) Size distribution measured by NTA for the sorafenib mass fractions as indicated on graph. (dilution factor: 20).

Then, we investigated the co-nanoprecipitation of the SPION with the drug both in the SFME and Ouzo domains. Briefly, the particles were mixed with the sorafenib in THF, then water was added rapidly to reach the final composition. After 6 hours, a copolymer poly(ethylene glycol)-*b*-(acrylic acid) (PEG<sub>7k</sub>-PAA<sub>2k</sub>) is added. The role of the polymer is twofold. It is both to cross-link the SPION and to ensure the colloidal stability of the capsules.<sup>7</sup> Finally, the solvent was evaporated and the suspensions purified by magnetic separation (only the capsules are attracted by the magnet), followed by redispersion of the pellet in water. Analyzing different compositions in sorafenib with NTA clearly evidences two populations of capsules differing by their sizes, either  $\sim 80$  nm or  $\sim 150$  nm (Figure 4). At mass fraction  $2.3 \times 10^{-5}$ , only the large capsules are observed. When increasing the amount of sorafenib, this population decreases progressively in favor of the population of smaller capsules. Finally, in the Ouzo domain the size distributions of the hybridosomes are significantly narrower than the corresponding drug nanoprecipitate in the absence of SPION (Figure SI-1b). The size-focusing effect of the SPION in the Ouzo domain is due to the arrested coalescence of the emulsion droplets in the

presence of nanoparticles.<sup>23</sup> More surprisingly, in the SFME domain we found capsules with a broader mean size and dispersity than the drug nanoprecipitate in the absence of SPION, as shown in Figure SI-1a. This swelling occurs after addition of the SPION but prior to the addition of the polymer and solvent evaporation, as shown by the NTA analysis (Figure SI-2). It can be hypothesized that this is due to the presence of free octylamine and oleic acid, which are introduced as the ligands of the SPION. Indeed, these ligands are only weakly bound to the SPION and in dynamic equilibrium with the liquid phase. Assuming that all the ligand used in the synthesis is present, we find a maximum total mass fraction of ligand of  $2.5 \cdot 10^{-4}$ , exceeding that of sorafenib. This amount is largely overestimated since (i) the particles are purified by magnetic sorting and (ii) a fraction of the ligand is adsorbed at the surface of the SPION. To clarify the possible role of the ligands, we investigated the phase diagram formed by an equimolar mixture of octylamine and oleic acid in a range of water/THF compositions (from the THF mass fraction 0.1 to 0.4). This diagram (Figure SI-3), shows the presence of an Ouzo domain. However, the composition corresponding to the maximal (overestimated) amount of ligand (indicated by a red mark) lies close but outside of this Ouzo domain. In addition, we observed that SPION capsules are not observed in the absence of solute. In summary, in the range of concentrations used, the ligands themselves do not form an Ouzo domain nor allow the formation of capsules, but they may swell the sorafenib core and modify the chemical equilibria at play in the SFME.

**3.2 Case of sorafenib tosylate salt.** Our purpose here is to compare the behavior of the salt to that of the molecular form. We first determined the stability limit of the tosylate form in the water:THF mixture, using SMLS (Figure SI-4). Interestingly, it is found identical, in terms of molar fraction, to that of the molecular form ( $\phi_{\text{soraf}} = \sim 6 \cdot 10^{-6}$ ). However, the evolution of the droplet size with the drug concentration is very different for the two forms. Indeed, in the range of the concentration investigated, it is almost constant (in the range 120-140 nm) for the salt, whereas it increases from ca 60 nm up to 180 nm for the molecular form.

Regarding surface charge, we observe that the droplets of both forms are negatively charged at all concentrations, as shown by measurements of the electrophoretic mobility (Figure 5b). For the molecular form (dashed line in Fig 5b), the surface charge increases (in absolute values) in the range of molar fractions  $2 \cdot 10^{-6}$  -  $10^{-5}$ , that is close to the SFME-Ouzo transition. This surface-charging effect at the Ouzo transition was observed previously with other molecular systems<sup>19</sup> and is attributed to the adsorption of carboxylate or hydroxyl ions when the droplets contain more solute (and less solvent).<sup>39-41</sup> In contrast, the charge is almost constant for the tosylate form within the same range of compositions (molar fractions  $2 \cdot 10^{-6}$  to  $10^{-5}$ , solid line in Fig 4b). It is important to note here, that the measurement of the hydrodynamic diameter of a colloid takes into account the possible ionic corona, such that increasing the surface charge of a colloid increases its hydrodynamic diameter. However, in the case of the molecular form of sorafenib, the increase of size with the drug concentration is also confirmed by i) the decrease of the optical transmission of the samples, ii) the broadening of their size distribution, and iii) their colloidal instability. In summary, the present

results suggest that the size and charge of the tosylate form is less affected by concentration than these of the molecular form.

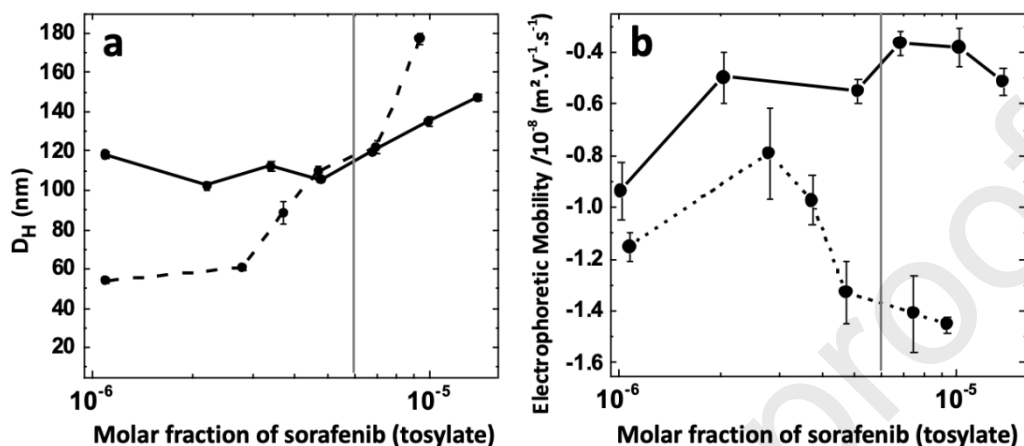


Figure 5: Comparison of the molecular and ionic forms of sorafenib in the water/THF/sorafenib (or sorafenib tosylate) systems: (a) mean value of the hydrodynamic diameter; (b) electrophoretic mobility. Dashed line: sorafenib; Full line: sorafenib tosylate. Vertical line: solubility limit determined by SMLS method.

We tried to prepare nanocapsules from the tosylate salt of sorafenib, similarly as for the molecular form. In the Ouzo domain, capsules of several microns were observed, whereas small capsules were observed in the SFME domain. More precisely, the NTA of the dispersions shows mainly sizes of the order of 100-200 nm for solute concentrations below mass fraction  $7 \times 10^{-5}$  and a broad distribution beyond (Figure 6d). This is confirmed by TEM analyses (Figure 6 a-c), although a few very large capsules are also visible at the low concentrations (not shown). This contrasts with the case of molecular sorafenib, which shows the opposite trend. We do not have a clear explanation for this, but an interaction between the tosylate and the oleylamine coating the SPION may be at play. In any case, it is important to note that capsules could be obtained with both forms, but in different conditions.

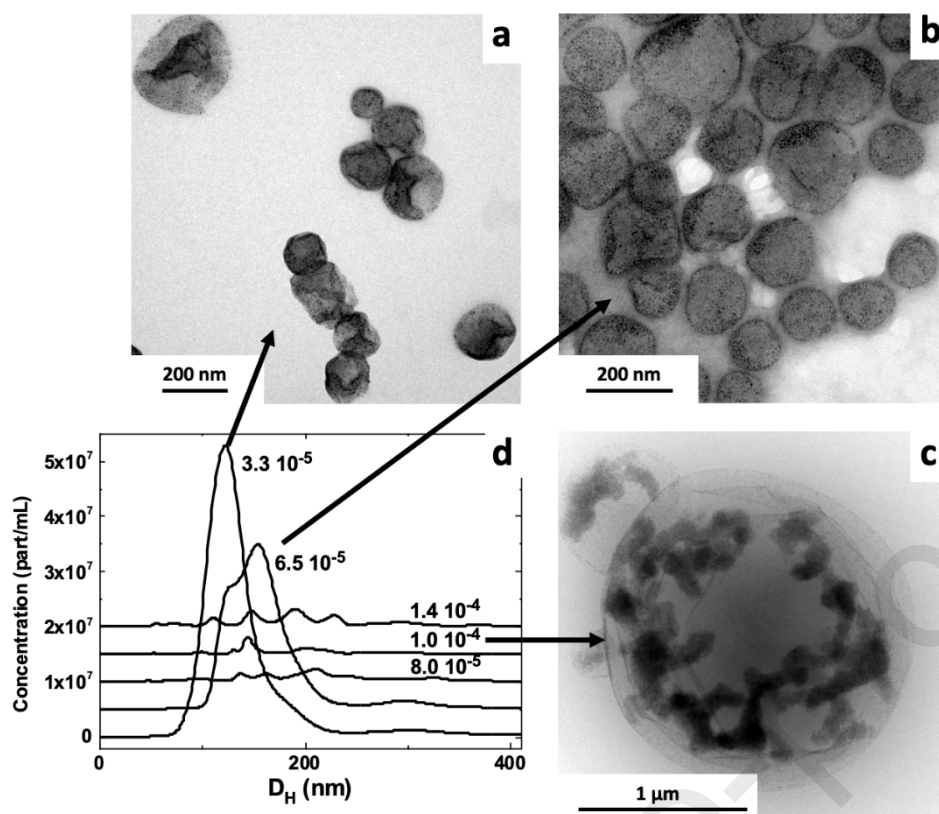


Figure 6: Characterization of sorafenib tosylate-SPION nanocapsules. (a-c) TEM pictures of the capsules for three mass fractions of sorafenib tosylate:  $3.3 \times 10^{-5}$ ;  $6.5 \times 10^{-5}$ ;  $1.0 \times 10^{-4}$ ; (d) Size distribution measured by NTA for the mass fractions indicated on graph.

The magnetic sorting is a convenient way to separate the drug incorporated into the SPION capsules from the continuous phase. Any particle of drug nanoprecipitated outside the capsules will also remain in the supernatant. This allowed us to quantify the encapsulation yield, for various compositions both in the SFME and Ouzo domains, by HPLC measurements of the amount of sorafenib in the supernatants. In all cases, the measured encapsulation yield is close to 85% (Table SI-2). This may seem surprising for samples in the SFME, since in this domain the sorafenib concentration is less than the solubility limit ( $1.2 \times 10^{-4}$  at  $\phi_{\text{THF}} = 0.23$ ). However, the encapsulation yield is measured after the evaporation of the solvent. Therefore, the sorafenib may concentrate in the core of the capsules, which are permeable,<sup>42</sup> during the evaporation step. We then monitored the release rate of sorafenib, after dispersion of the purified capsules in water (Figure 7). Release is very low during the first 5 days, then starts to increase. This phenomenon may be related to the slow formation of crystals, that can be observed visually a few days after the formation of the capsules. Indeed, sorafenib is poorly soluble in water. It might first nanoprecipitate as an amorphous form, but later reorganizes into crystals that are more thermodynamically stable. Thus, if crystals nucleate, they will eventually form macroscopic crystals, draining out the sorafenib from the capsules.

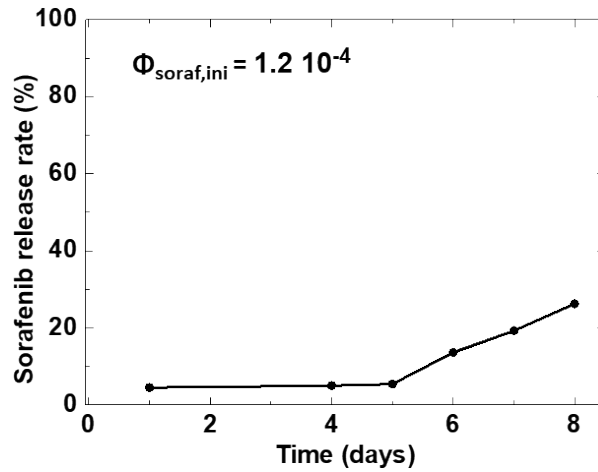


Figure 7: Kinetics of release of encapsulated sorafenib ( $\varphi_{soraf,initial} = 1.2 \cdot 10^{-4}$ )

**3.3 Case of a liquid solute:  $\alpha$ -tocopherol.** To further study the influence of the physical properties of the solute, we selected  $\alpha$ -tocopherol as an example of liquid solute to form the organic core of the hybridosomes. Indeed, the solid vs liquid nature of the solute may be a determinant parameter for the formation of the capsules, since it may affect the interaction of the particles with the underlying phase as well as their motion dynamics.

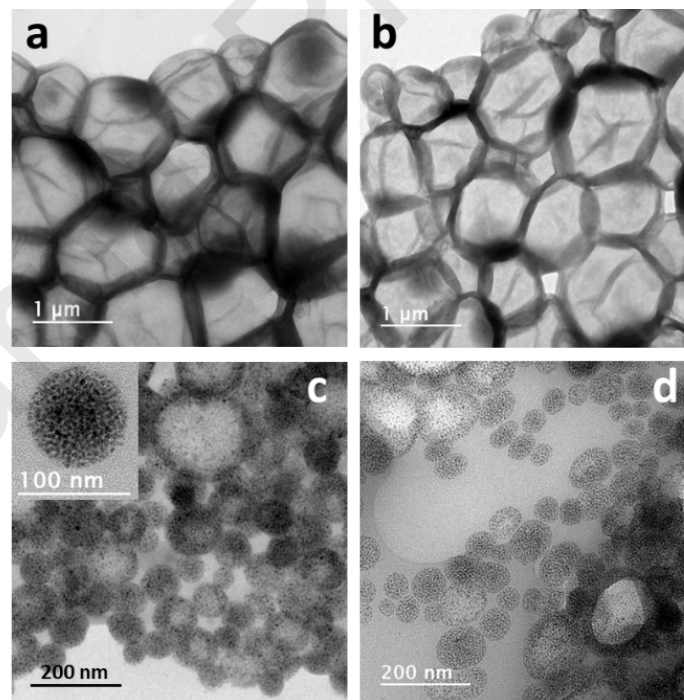


Figure 8: TEM images of  $\alpha$ -tocopherol-SPION hybridosomes obtained from compositions in the SFME domain with mass fraction of  $\alpha$ -tocopherol (a)  $5.0 \cdot 10^{-8}$  (b)  $1.0 \cdot 10^{-6}$ , and in the Ouzo domain (c)  $1.0 \cdot 10^{-5}$  and (d)  $5.0 \cdot 10^{-5}$ .

The diagram water/THF/ $\alpha$ -tocopherol was investigated in detail elsewhere.<sup>19</sup> Here, we tried to elaborate hybridosomes from various compositions, both in the SFME and Ouzo domains keeping the amounts of particles and polymer the same as in the case of sorafenib. Capsules can be formed from both the SFME and Ouzo domains as shown by TEM (Figure 8). The size dispersions of the hybridosomes were also analyzed by NTA (Figure SI-5). We observed that capsules prepared from the Ouzo domain are mainly less than 100 nm. Their dispersions exhibit remarkably narrow sizes distribution, except for the most concentrated sample, that lays close to the spinodal line. In contrast, in the SFME domain, the capsule sizes exceed 1  $\mu$ m and could not be analyzed by NTA. Finally, it is remarkable here that both liquid and solid molecular solutes show the same behavior and allow to form hybridosomes from any composition in the Ouzo domain.

**3.4 Case of paclitaxel.** The case of paclitaxel is different from the previous examples. Indeed, only two types of samples were found: either fully limpid, or containing macroscopic crystals (Figure 9). The two corresponding domains are separated by a straight line in the semi-Log representation, most probably corresponding to the binodal curve. Indeed, the extrapolation of this line to pure water (*i.e.* 0% THF) is consistent with the solubility limit given in the literature ( $S = 6.5 \cdot 10^{-6}$  M or equivalently a mass fraction of  $5.5 \cdot 10^{-6}$ ). Therefore, this system shows no Ouzo domain. However, on the left side of the binodal we observed a SFME. Indeed, the NTA reveals the presence of a population of droplets of well-defined size (see for instance Figure SI-6, which shows a narrow size distribution with a main mode at  $42.5 \pm 1.5$  nm). In addition, the SMLS analysis (Figure SI-7) confirms the stability of these compositions.

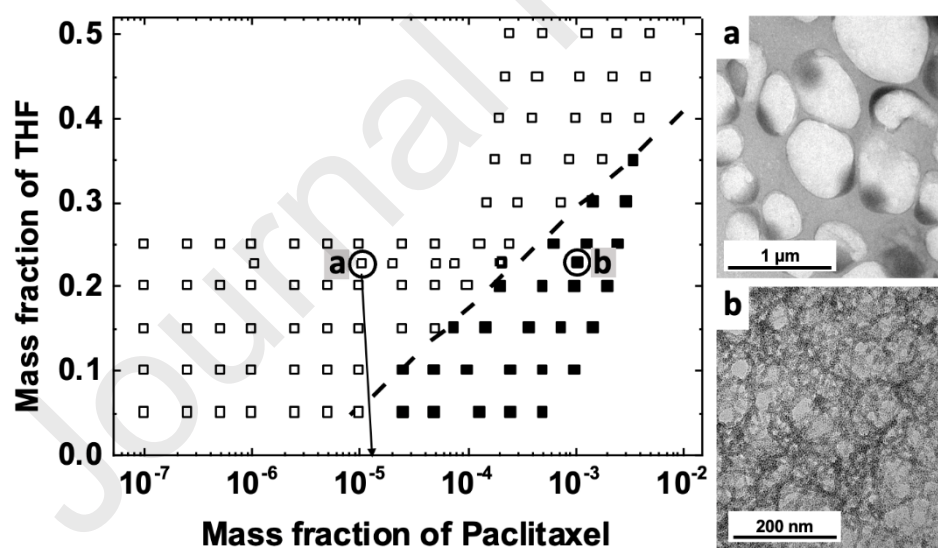


Figure 9: Phase diagram of the system water/THF/paclitaxel (Empty squares: homogeneous samples; full squares: crystals), and TEM micrographs for samples nanoprecipitated in the presence of SPION, prepared from the compositions a, and b (prior to evaporation of the THF). The arrow shows the change of solvent composition during evaporation.

Next, we investigated the possibility to elaborate capsules from compositions in the SFME domain as well as beyond the binodal (Figure 9). To this aim, the compositions were nanoprecipitated in the presence of SPION. Like in the absence of the SPION, no crystals were observed on the left side of the binodal (for instance point a in the Figure 9), whereas the formation of Paclitaxel crystals was observed beyond the binodal curve (for instance point b in Figure 9). Figure 9a and b show TEM images of samples prepared from compositions setting on the left and right side of the binodal, respectively. Capsules with size below 1  $\mu\text{m}$  were observed (Figure 9), but only on the left side of the binodal where organic particles can form the core. Then the THF of all SFME samples was removed by evaporation. This changes the solvent composition, and causes the formation of crystals, as the solubility limit is overpassed. Interestingly, it is not the case for the lowest composition (point a), despite the fact that the amount of paclitaxel exceeds its solubility in water (see arrow in Figure 9). Closer to the binodal curve (sample b) larger capsules are formed (Figure 9a).

### 3.4 In vitro evaluation of the chemotherapeutic efficacy of sorafenib encapsulated in hybridosomes

To ensure that the capsules themselves were not toxic, we incubated HuH7 cells for 48 h with a solution of hybridosomes made from SPIONs, without drug (Figure 10f). In this case, the concentrations were chosen such as to keep the same amount of capsules (in terms of [Fe]) as that used to determine the  $\text{IC}_{50}$  of sorafenib-loaded hybridosomes. Hybridosomes alone present a negligible effect on the viability of HuH7 cells after 48 h of incubation ( $\text{IC}_{50}=98.0 \pm 1.7\mu\text{M}$ ). Finally, the cytotoxicity of the different products used to produce hybridosomes was evaluated (Figure SI-8). Even at the highest concentration tested (25 mM), which was itself much higher than the synthesis conditions, no cytotoxicity was observed.

To evaluate the chemotherapeutic efficacy of encapsulated sorafenib, we performed cell viability tests over 48 hours on HuH7-LUC cell lines (Figure 10). The results are summarized in Table 1. Sorafenib and sorafenib tosylate dissolved in DMSO were used as positive controls. They both yield an  $\text{IC}_{50}$  value (13.0  $\mu\text{M}$ ) close to that reported in previous studies on HuH7 cell line.<sup>43</sup> Sorafenib, whether free or nanoprecipitated in hybridosomes, presents the same toxicity. Indeed, the two formulations present similar curve profiles and close  $\text{IC}_{50}$  values, that of encapsulated sorafenib being slightly higher (19.0  $\mu\text{M}$ ). It cannot be ruled out that some of the sorafenib remains trapped by the polymer used to cross-link the shell of nanoparticles, and therefore is not redistributed to the cells, explaining an apparent lower toxicity. Interestingly, drug-free hybridosomes exhibit a very different curve profile compared to that of sorafenib (Figure 10c) or sorafenib loaded-hybridosomes (Figure 10e). This unambiguously demonstrates that the toxicity of sorafenib encapsulated in hybridosomes is due to the sorafenib and not to the capsules.

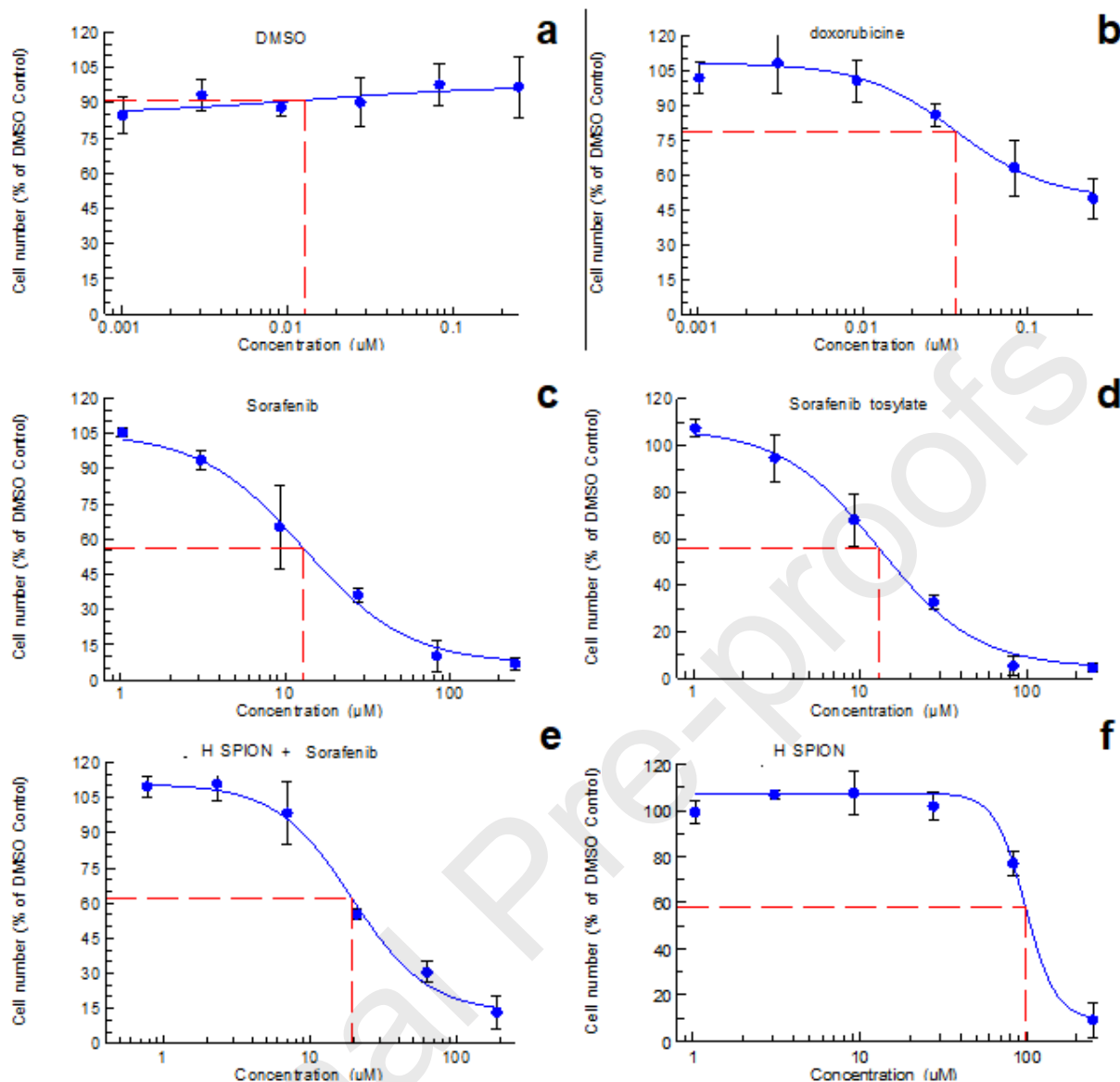


Figure 10: Cellular viability of HuH7-LUC cells after 48 h incubation in presence of (a) DMSO (negative control), (b) doxorubicin (positive control), (c) sorafenib, (d) sorafenib tosylate, (e) sorafenib loaded hybridosomes (f), hybridosomes formulated without sorafenib (BHT as organic core). Since no drug is used in this case, the concentration axe is calculated to represent the same amount of hybridosomes as used for comparable values in (e).

**Table 1** 50% inhibitory concentration (IC<sub>50</sub>) of sorafenib formulated or not in hybridosomes and controls.

Drug	Sorafenib tosylate	Sorafenib	Hybridosomes	Hybridosomes loaded with sorafenib
IC <sub>50</sub> (μM)	13.0 ± 1.6	13.0 ± 1.7	98.0 ± 1.6	19.0 ± 2.6

#### 4. Conclusion

We report for the first time the synthesis of hybridosomes with a core made of drug only. This is achieved through a one-pot co-nanoprecipitation process. We investigated the encapsulation of four molecules, including the approved anticancer drugs sorafenib and

paclitaxel, with similar solubility properties but differing by their physical state (solid vs liquid) or chemical structure (molecular vs salt). Following a rational strategy, we first identified the water/THF/drug compositions forming an organic core, either as an Ouzo emulsions or a SFME. Then, we investigated the effect of the SPION on the size and stability of the nanoprecipitate. Our main findings are that: (1) capsules are equally prepared using liquid ( $\alpha$ -tocopherol) or solid drugs (sorafenib). (2) The crystallization of the molecule may hinder encapsulation because it drains the nanoprecipitate out of the capsule core (case of paclitaxel). This issue may be solved in future works by using an additional polymer coating, using preferably a biodegradable polymer to allow release of the drug. (3) It appeared more interesting to encapsulate the molecular form of sorafenib rather than the corresponding tosylate salt, since small capsules are obtained at most concentrated composition for the molecular form. Indeed, for the molecular form, samples prepared in the Ouzo domain (preferably close to the binodal) yielded capsules of ca 80 nm in diameter. (4) Sorafenib-loaded hybridosomes show a chemotherapeutic activity comparable to that of the free drug, showing the availability of the encapsulated drug *in vitro*. In addition, the encapsulation efficiency is very high (around 80%), meaning that the loss of drug during the process remains low. Finally, the co-nanoprecipitation strategy presented here proves both simple to implement and highly effective for encapsulating drugs and, more generally, a wide variety of hydrophobic compounds.

**Acknowledgements.** The authors wish to thank L. Rault (Themis) and A. Burel and A. Dupont (MRic TEM, UAR Blosit) for transmission electron microscopy analysis. The authors also thank H. Solhi (ImPACcell, UAR Blosit) for the cytotoxicity studies. This work was supported by the University of Rennes, the Centre National de la Recherche Scientifique (CNRS) and the ANR. We also acknowledge financial support from ITMO Cancer of Aviesan within the framework of the 2021-2030 Cancer Control Strategy, on funds administered by Inserm.

1. Liu, Y. *et al.* Stable Polymer Nanoparticles with Exceptionally High Drug Loading by Sequential Nanoprecipitation. *Angew. Chem. Int. Ed.* **59**, 4720–4728 (2020).
2. Wilhelm, S. *et al.* Analysis of nanoparticle delivery to tumours. *Nat Rev Mater* **1**, 16014 (2016).
3. Hoshyar, N., Gray, S., Han, H. & Bao, G. The effect of nanoparticle size on *in vivo* pharmacokinetics and cellular interaction. *Nanomedicine* **11**, 673–692 (2016).
4. Mitchell, M. J. *et al.* Engineering precision nanoparticles for drug delivery. *Nat Rev Drug Discov* **20**, 101–124 (2021).

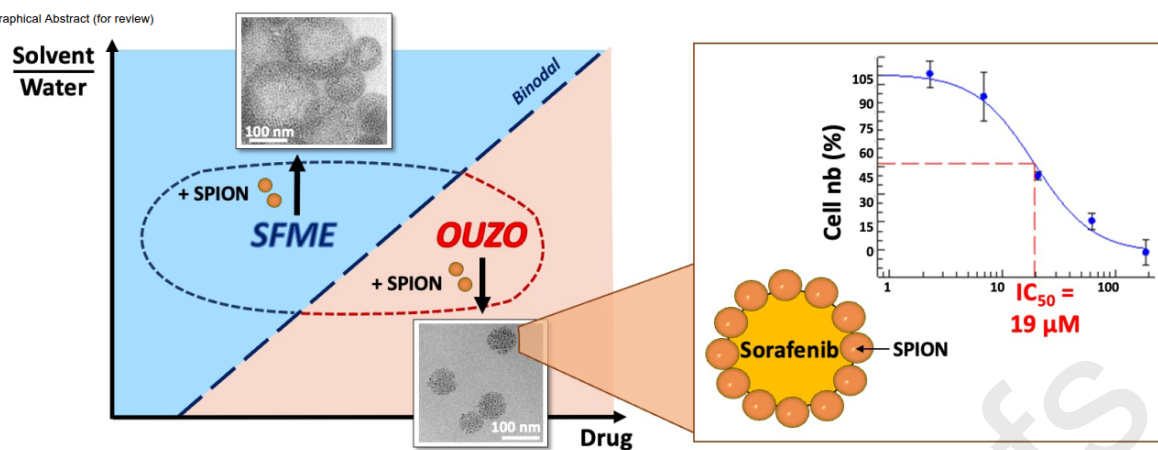
5. Huang, P. *et al.* Biodegradable Gold Nanovesicles with an Ultrastrong Plasmonic Coupling Effect for Photoacoustic Imaging and Photothermal Therapy. *Angewandte Chemie International Edition* **52**, 13958–13964 (2013).
6. Liu, Y. *et al.* Folding Up of Gold Nanoparticle Strings into Plasmonic Vesicles for Enhanced Photoacoustic Imaging. *Angewandte Chemie International Edition* **54**, 15809–15812 (2015).
7. Sciortino, F. *et al.* Simple Engineering of Polymer-Nanoparticle Hybrid Nanocapsules. *ChemNanoMat* **2**, 796–799 (2016).
8. Goubault, C. *et al.* Radiosensitizing Fe-Au nanocapsules (hybridosomes<sup>®</sup>) increase survival of GL261 brain tumor-bearing mice treated by radiotherapy. *Nanomedicine: Nanotechnology, Biology and Medicine* **40**, 102499 (2022).
9. Ramos, R. *et al.* Nanocapsules Produced by Nanoprecipitation of Designed Suckerin-Silk Fusion Proteins. *ACS Macro Lett.* **10**, 628–634 (2021).
10. Yan, X., Bernard, J. & Ganachaud, F. Nanoprecipitation as a simple and straightforward process to create complex polymeric colloidal morphologies. *Advances in Colloid and Interface Science* **294**, 102474 (2021).
11. Goubault, C. *et al.* The Ouzo effect: A tool to elaborate high-payload nanocapsules. *Journal of Controlled Release* **10**, 430–439 (2020).
12. Vitale, S. A. & Katz, J. L. Liquid Droplet Dispersions Formed by Homogeneous Liquid-Liquid Nucleation: “The Ouzo Effect”. *Langmuir* **19**, 4105–4110 (2003).
13. Beck-Broichsitter, M., Rytting, E., Lebhardt, T., Wang, X. & Kissel, T. Preparation of nanoparticles by solvent displacement for drug delivery: A shift in the “ouzo region” upon drug loading. *European Journal of Pharmaceutical Sciences* **41**, 244–253 (2010).

14. Pucci, C., Cousin, F., Dole, F., Chapel, J.-P. & Schatz, C. Impact of the Formulation Pathway on the Colloidal State and Crystallinity of Poly- $\epsilon$ -caprolactone Particles Prepared by Solvent Displacement. *Langmuir* **34**, 2531–2542 (2018).
15. Beck-Broichsitter, M. Stability-limit ‘Ouzo region’ boundaries for poly(lactide- co - glycolide) nanoparticles prepared by nanoprecipitation. *International Journal of Pharmaceutics* **511**, 262–266 (2016).
16. Bassani, D. M., Carteau, D., Pianet, I., Brunerie, P. & Guillemat, B. Probing the Initial Events in the Spontaneous Emulsification of *trans* -Anethole Using Dynamic NMR Spectroscopy. *Langmuir* **23**, 3561–3565 (2007).
17. Roger, K., Botet, R. & Cabane, B. Coalescence of Repelling Colloidal Droplets: A Route to Monodisperse Populations. *Langmuir* **29**, 5689–5700 (2013).
18. Vratsanos, M. A., Xue, W., Rosenmann, N. D., Zarzar, L. D. & Gianneschi, N. C. Ouzo Effect Examined at the Nanoscale via Direct Observation of Droplet Nucleation and Morphology. *ACS Cent. Sci.* **9**, 457–465 (2023).
19. Iglicki, D., Goubault, C., Nour Mahamoud, M., Chevance, S. & Gauffre, F. Shedding light on the formation and stability of mesostructures in ternary “Ouzo” mixtures. *Journal of Colloid and Interface Science* **633**, 72–81 (2023).
20. Ganachaud, F. & Katz, J. L. Nanoparticles and Nanocapsules Created Using the Ouzo Effect: Spontaneous Emulsification as an Alternative to Ultrasonic and High-Shear Devices. *ChemPhysChem* **6**, 209–216 (2005).
21. Yan, X. *et al.* Simple but Precise Engineering of Functional Nanocapsules through Nanoprecipitation. *Angew. Chem.* 7030–7033 (2014).
22. Aschenbrenner, E. *et al.* Using the Polymeric Ouzo Effect for the Preparation of Polysaccharide-Based Nanoparticles. *Langmuir* **29**, 8845–8855 (2013).

23. Goubault, C. *et al.* Effect of nanoparticles on spontaneous Ouzo emulsification. *Journal of Colloid and Interface Science* **603**, 572–581 (2021).
24. Bago Rodriguez, A. M. & Binks, B. P. Capsules from Pickering emulsion templates. *Current Opinion in Colloid & Interface Science* **44**, 107–129 (2019).
25. Hazt, B. *et al.* Unconventional and conventional Pickering emulsions: Perspectives and challenges in skin applications. *International Journal of Pharmaceutics* **636**, 122817 (2023).
26. Sciortino, F. *et al.* Structure and elasticity of composite nanoparticle/polymer nanoshells (hybridosomes<sup>®</sup>). *Soft Matter* **13**, 4393–4400 (2017).
27. Lepeltier, E., Bourgaux, C. & Couvreur, P. Nanoprecipitation and the “Ouzo effect”: Application to drug delivery devices. *Advanced Drug Delivery Reviews* **71**, 86–97 (2014).
28. Yan, X. *et al.* Modular construction of single-component polymer nanocapsules through a one-step surfactant-free microemulsion templated synthesis. *Chemical Communications* **53**, 1401–1404 (2017).
29. Casterou, G. *et al.* Improved Transversal Relaxivity for Highly Crystalline Nanoparticles of Pure  $\gamma$ -Fe<sub>2</sub>O<sub>3</sub> Phase. *Chem. Eur. J.* **21**, 18855–18861 (2015).
30. Mahendra, N. R., Das, B. & Hazra, D. K. Densities and viscosities of the binary aqueous mixtures of tetrahydrofuran and 1,2-dimethoxyethane at 298, 308 and 318 K. *INDIAN J. CHEM. TECHNOL.* **5** (1994).
31. Sebaugh, J. L. Guidelines for accurate EC<sub>50</sub>/IC<sub>50</sub> estimation. *Pharmaceut. Statist.* **10**, 128–134 (2011).
32. Drugbank.

33. Lögers Michael *et al.* process for the production of 4-[4-[[4-Chloro-3-(trifluoromethyl)phenyl]amino}carbonyl]amino]phenoxy}-N-methylpyridine-2-carboxamide. (2006).
34. Jagdev Singh Jaryal, Swargam Sathyanarayana, Rajesh Kumar Thaper, & Mohan Prasad. Process for the preparation of sorafenib tosylate. (2011).
35. *Nexavar : EPAR - product information.* [www.ema.europa.eu/en](http://www.ema.europa.eu/en) (2009).
36. *Sorafenib Accord : EPAR- Product information.* <https://www.ema.europa.eu/en> (2022).
37. Wang, X. *et al.* Bioavailability and pharmacokinetics of sorafenib suspension, nanoparticles and nanomatrix for oral administration to rat. *International Journal of Pharmaceutics* **419**, 339–346 (2011).
38. Li, X. *et al.* Formulation and pharmacokinetic evaluation of a paclitaxel nanosuspension for intravenous delivery. *IJN* 1497 (2011) doi:10.2147/IJN.S21097.
39. Roger, K. & Cabane, B. Why Are Hydrophobic/Water Interfaces Negatively Charged? *Angewandte Chemie International Edition* **51**, 5625–5628 (2012).
40. Jena, K. C., Scheu, R. & Roke, S. Surface Impurities Are Not Responsible For the Charge on the Oil/Water Interface: A Comment. *Angew. Chem. Int. Ed.* **51**, 12938–12940 (2012).
41. Ganachaud, F. *et al.* Central Role of Bicarbonate Anions in Charging Water/Hydrophobic Interfaces. *J. Phys. Chem. Lett.* **9**, 96–103 (2018).
42. Sciortino, F. *et al.* Structure and elasticity of composite nanoparticle/polymer nanoshells (hybridosomes®). *Soft Matter* **13**, 4393–4400 (2017).
43. Li, H., Xu, K., Pian, G. & Sun, S. Artesunate and sorafenib: Combinatorial inhibition of liver cancer cell growth. *Oncol Lett* (2019) doi:10.3892/ol.2019.10810.

Graphical Abstract (for review)



**HIGHLIGHTS**

- A one step method to elaborate drug capsules (100 nm) coated with nanoparticles is reported
- The nanoprecipitation diagram of the drug is a useful guide to form capsules
- The molecular form of sorafenib yields submicronic capsules in the Ouzo domain
- Sorafenib tosylate yields submicronic capsules from the Surfactant Free Microemulsion domain
- The final size of the capsule depends on the overall composition and solute molecular structure
- Monodispersed capsules (~80 nm) can be formed close to the Ouzo boundary.
- Encapsulation efficiency greater than 80% is reached
- The encapsulated drug therapeutic activity is preserved (*in vitro*).

**Declaration of interests**

The authors declare that they have no known competing financial interests or personal relationships that could have appeared to influence the work reported in this paper.

The authors declare the following financial interests/personal relationships which may be considered as potential competing interests:

Journal Pre-proofs